Subdivision-Based Mesh Convolution Networks

SHI-MIN HU, Tsinghua University, China
ZHENG-NING LIU, Tsinghua University, China
MENG-HAO GUO, Tsinghua University, China
JUN-XIONG CAI, Tsinghua University, China
JIAHUI HUANG, Tsinghua University, China
TAI-JIANG MU, Tsinghua University, China
RALPH R. MARTIN, Cardiff University, UK and Tsinghua University, China
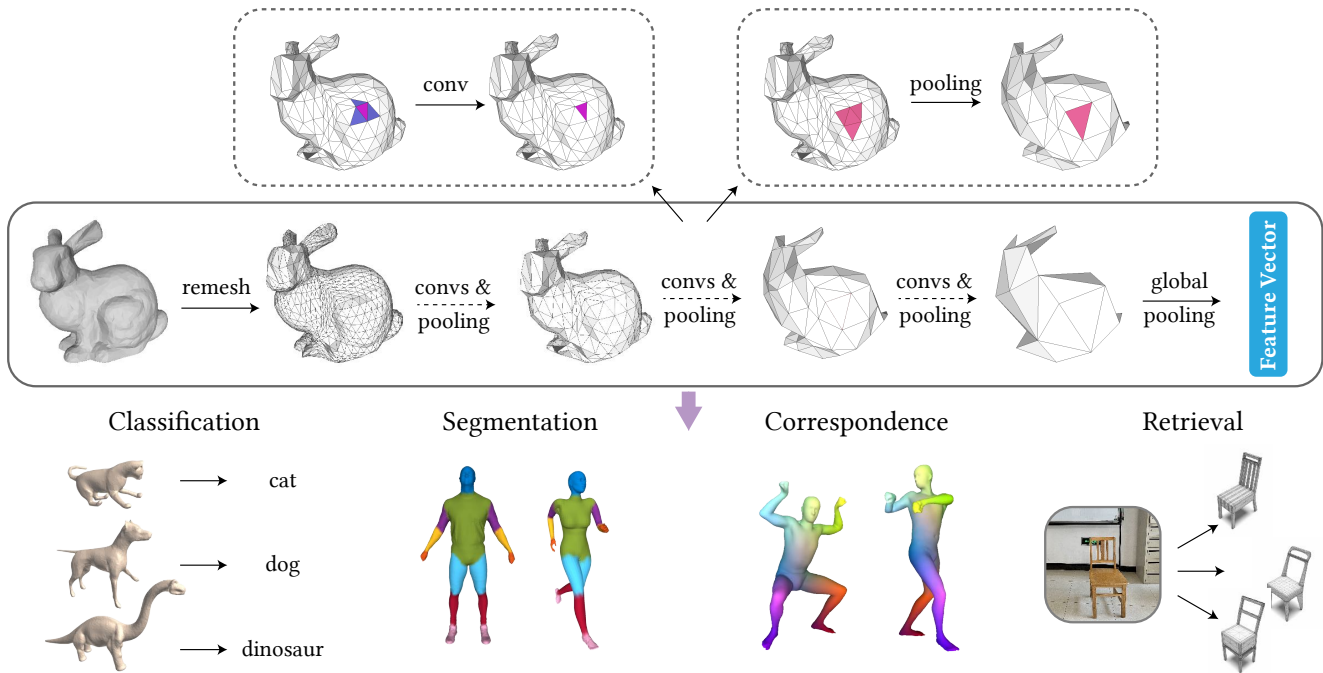
Fig. 1. The pipeline of SubdivNet, a subdivision-based mesh convolution network for deep geometric learning. Given a mesh as input, we build a hierarchical subdivision structure with a pyramid of regular connectivities, analogous to a 2D image pyramid. We show that such a structure leads to natural notions of convolution, pooling, and upsampling operations on the 3D meshes, which together act as the building blocks for our mesh-based deep neural network, SubdivNet. We show by various applications that our network is effective and efficient for mesh-based representation learning.

Authors' addresses: Shi-Min Hu, Tsinghua University, Beijing, China, shimin@tsinghua.edu.cn; Zheng-Ning Liu, Tsinghua University, Beijing, China, lzhengning@gmail.com; Meng-Hao Guo, Tsinghua University, Beijing, China, gmh20@mails.tsinghua.edu.cn; Jun-Xiong Cai, Tsinghua University, 30 Shuangqing Rd, Haidian Qu, Beijing Shi, China, caijunxiong000@163.com; Jiahui Huang, Tsinghua University, 30 Shuangqing Rd, Haidian Qu, Beijing Shi, China, huang-jh18@mails.tsinghua.edu.cn; Tai-Jiang Mu, Tsinghua University, 30 Shuangqing Rd, Haidian Qu, Beijing Shi, China, taijiang@tsinghua.edu.cn; Ralph R. Martin, Cardiff University, South Glamorgan, UK, Tsinghua University, 30 Shuangqing Rd, Haidian Qu, Beijing Shi, China, MartinRR@cs.cf.ac.uk.

Convolutional neural networks (CNNs) have made great breakthroughs in 2D computer vision. However, the irregular structure of meshes makes it hard to exploit the power of CNNs directly. A subdivision surface provides a hierarchical multi-resolution structure, and each face in a closed 2-manifold triangle mesh is exactly adjacent to three faces. Motivated by these two properties, this paper introduces a novel and flexible CNN framework, named *SubdivNet*, for 3D triangle meshes with Loop subdivision sequence connectivity. Making an analogy between mesh faces and pixels in a 2D image allows us to present a mesh convolution operator to aggregate local features from adjacent faces. By exploiting face neighborhoods, this convolution can support standard 2D convolutional network concepts, e.g. variable kernel size, stride, and dilation. Based on the multi-resolution hierarchy, we propose a spatial uniform pooling layer which merges four faces into one and an upsampling method which splits one face into four. As a result, many popular 2D CNN architectures can be readily adapted to processing 3D meshes. Meshes with arbitrary connectivity can be remeshed to hold Loop subdivision sequence connectivity via self-parameterization, making SubdivNet a

general approach. Experiments on mesh classification, segmentation, correspondence, and retrieval from the real-world demonstrate the effectiveness and efficiency of SubdivNet.

CCS Concepts: • **Computing methodologies → Neural networks**; **Shape analysis**.

Additional Key Words and Phrases: Geometric Deep Learning, Convolutional Neural Network, Subdivision Surfaces, Mesh Processing

1 INTRODUCTION

The great success of deep convolutional neural networks (CNNs) in 2D computer vision has led to their generalisation to various disciplines, including 3D geometry. PointNet [Qi et al. 2017a] is a pioneering and successful approach for learning a feature representation of a point cloud. This has inspired researchers to find more powerful networks [Li et al. 2018; Qi et al. 2017b]; apart from point clouds, 3D geometry learning has been extended to other forms of 3D data, such as voxels [Klokov and Lempitsky 2017; Wang et al. 2017] and meshes [Hanocka et al. 2019; Lahav and Tal 2020].

In this paper, we consider 3D geometry learning using a mesh representation. Polygonal meshes are one of the most common representations for 3D data, being widely used in modeling, rendering, animation, 3D printing, etc. Unlike a point cloud, meshes has topological information. Compared to voxels, mesh represents geometric context more effectively, since it only represents the boundary of an object, and does not have redundant elements representing the object's interior.

Underpinning the success of 2D CNNs in the image domain is the inherently regular and hierarchical structure of images, which is beneficial to the formation of an image pyramid. This allows convolutional neural networks to explore features of different sizes by downsampling and upsampling. However, an arbitrary mesh is irregular and lacks the gridded arrangement of pixels in images, making it difficult to define a standard 2D convolution with variable kernel size, stride, and dilation. This in turn prevents the 3D geometry learning methods from taking advantage of the mature designs of network architecture used in the image domain. Furthermore, the unstructured connectivity between vertices and faces precludes finding a simple fine-to-coarse structure for meshes. One may consider levels of detail (LOD) via mesh simplification, but the mapping of geometry primitives between each level is not uniquely defined, and we cannot derive an intuitive pooling operator in an LOD hierarchy. To apply the power of CNNs to meshes, efforts have been made to define special convolution operations on the surfaces of shapes, analogously to 2D images. Such methods usually try to encode or resample the neighborhood of a vertex into a regular local domain [Boscaini et al. 2016; Maron et al. 2017; Masci et al. 2015; Monti et al. 2017; Poulenard and Ovsjanikov 2018; Tatarchenko et al. 2018], where the convolutional operation can be derived. Recently, special downsampling schemes have been proposed to dynamically merge regions (using edge collapse) [Hanocka et al. 2019; Milano

et al. 2020], but they do not provide uniform downsampling of a kind that can be used as a basic operation as in 2D CNNs. Although the attention mechanism [Velickovic et al. 2018] can be applied to capture global context by treating a mesh as a graph, it usually comes at the cost of heavy computation.

Instead, inspired by the image pyramids in 2D CNNs that allow local features to be aggregated into larger-scale features at different levels, we note that subdivision surfaces also construct well-defined hierarchical mesh pyramids. A subdivision surface is a smooth surface produced by refining a coarse mesh. In particular, in Loop subdivision [Loop 1987], each triangle mesh face is split into 4 triangles and then vertex positions are adjusted to smooth the new mesh (see Fig. 2(a)). As a result, the Loop subdivision scheme gives a 1-to-4 face mapping from the coarse mesh to the finer one. Correspondingly, if a mesh has the same connectivity as a Loop subdivision surface, it has a natural correspondence to a one-level-coarser mesh, and indeed, a carefully constructed Loop subdivision surface may preserve the Loop property over several levels leading to a fine to coarse hierarchy.

Furthermore, in any closed 2-manifold mesh, every face is exactly surrounded by 3 other faces. The fixed number of face neighbors suggests a regular structure analogous to that of pixels in images, which makes it ready for deriving a standard convolutional operation on meshes.

We use Loop subdivision sequence connectivity as a basis for *SubdivNet* which can learn feature representations for meshes with such connectivity. By carefully using the neighbors of faces, we define a novel convolutional operation on mesh faces; it allows variable kernel size, stride, and dilation; so that various popular convolutional operations on 2D pixel grids can readily be transferred to this domain. Thanks to the flexibility of our new convolutional operation on triangle meshes, successful neural networks in the image domain, such as ResNet [He et al. 2016], Deeplab v3+ [Chen et al. 2018], etc., can be naturally adapted to meshes, which is not the case for previous mesh convolution methods. Thus, unlike previous convolutions defined on meshes [Feng et al. 2019; Hanocka et al. 2019; Wang et al. 2018], ours can operate on a larger receptive field and is more capable of mesh feature learning.

SubdivNet requires a mesh with subdivision sequence connectivity as input, which may seem overly restrictive. Fortunately, a triangle mesh can be remeshed into one with this property via self-parameterization [Lee et al. 1998; Liu et al. 2020], which can be applied to any closed 2-manifold with arbitrary genus. As a result, SubdivNet can act as a general feature extractor for closed 2-manifold triangle meshes.

SubdivNet achieves state-of-the-art performance on 3D mesh tasks, e.g. mesh classification, segmentation, and shape correspondence. It can also be potentially employed to many other tasks, such as mesh registration, smoothing, and refinement.

In summary, our work makes the following contributions:

- a general mesh convolutional operation that permits variable kernel size, stride, and dilation analogous to standard 2D convolutions, making it possible to adapt well-known 2D CNNs to mesh tasks,

- SubdivNet, a general mesh neural network architecture based on mesh convolution and subdivision sequence connectivity, with uniform pooling and upsampling, for geometric deep learning, supporting dense prediction tasks,
- a demonstration that SubdivNet provides excellent results for various applications, such as shape correspondence and shape retrieval.

2 RELATED WORK

2.1 3D geometry learning in general

One way of applying deep learning to geometric data is to transform 3D shapes into images, e.g. , an unordered set of projections [Su et al. 2015], panoramas [Shi et al. 2015], or geometry images [Sinha et al. 2016], and run 2D CNNs on them. This family of *indirect* methods is sensitive to pose because an additional view-dependent projection step is involved. Another line of *direct* solutions are to represent the shapes in their intrinsic 3D space, such as volumetric data, whereupon 3D CNNs can be applied [Maturana and Scherer 2015; Wu et al. 2015] or adapted for higher resolution [Klokov and Lempitsky 2017; Liu et al. 2021; Wang et al. 2017]. Recently, point-based learning techniques have emerged [Li et al. 2018; Qi et al. 2017a,b; Wang et al. 2019] due to the ease of acquisition of point cloud data by 3D sensors. Nevertheless, the high computational demand for volumetric data and the lack of topological information for point clouds render current pipelines inefficient. Remarkably, methods which learn on *mesh surfaces* are free of the above problems and shown to be promising emerging directions. Readers are referred to recent surveys [Bronstein et al. 2017; Xiao et al. 2020] for a more comprehensive review on 3D geometry learning.

2.2 Deep learning on meshes

A mesh representation is based on three types of geometric primitive: vertices, edges, and faces. We classify mesh deep learning methods according to which of these is treated as the primary data.

2.2.1 Vertex based. One popular approach performs deep learning on 3D shapes by locally encoding in the neighborhood of each vertex into a regular domain, whereupon convolution operations (or kernel functions) can imitate those used for images. For example, Masci et al. [2015], Boscaini et al. [2016], and Monti et al. [2017] attempt to aggregate information in the pre-defined local patch. Chen et al. [2020] propose to unsupervisely learn a local convolutional template. Maron et al. [2017] and Haim et al. [2019] perform surface convolution using a global parameterization. Tatarchenko et al. [2018] propose to use planar convolution on the tangent image. Kostrikov et al. [2018] introduce the Dirac operator into graph neural networks. Poulenard et al. [2018] extend directional functions to surfaces, to maintain directional information as much as possible. To avoid possible loss of data fidelity when resampling, resampling-free neighborhood encoding is proposed by [Gong et al. 2019; Lim et al. 2018]. It serializes the neighbors of a vertex in a spiral manner, allowing efficient learning with LSTMs [Hochreiter and Schmidhuber 1997]. While methods of the above type are general, and allow varied mesh topology, with good local representation, they are usually less capable of learning the multi-scale and contextual information in a mesh.

Closer to our approach are methods with hierarchical design. Dilated kernel parametrization [Yi et al. 2017] and mesh downsampling and upsampling operations [Ranjan et al. 2018] are adopted in the spectral domain to define mesh convolution to aggregate multi-scale information. Schult et al. [2020] combine two kinds of convolutions separately defined on neighbors according to geodesic and Euclidean distance, also exploiting mesh simplification to provide a multi-resolution architecture. Based on subdivision sequence connectivity, our approach offers a more general and standard convolution directly defined on meshes; as such, it supports variable kernel size, stride, and dilation.

2.2.2 Edge based. In a 2-manifold mesh, every edge is adjacent to two faces, and the four other edges of those two triangles. This property is exploited by MeshCNN [Hanocka et al. 2019] to define an order invariant convolution. PD-MeshNet [Milano et al. 2020] does not require an assumption of edge manifoldness. It first constructs a primal graph and a dual graph from the input mesh, then performs convolutions on these graphs using a graph attention network [Monti et al. 2018; Velickovic et al. 2018]. Instead of exploiting regular neighborhood structures, MeshWalker [Lahav and Tal 2020] employs random walks along edges to extract shape features.

MeshCNN and PD-MeshNet dynamically contract edges to simplify meshes within the network, with ad-hoc rules, and MeshWalker uses variable steps of walk to build the hierarchy. Unlike our approach, they do not provide uniform downsampling for generic mesh convolutions, which has proven so successful in 2D CNNs.

2.2.3 Face based. Face based methods focus on how to efficiently and effectively gather information from neighboring faces. Xu et al. [2017] propose a rotationally-invariant face based method considering k-ring neighbors, guided by face curvature, to define convolution on meshes. Lian et al. [2019] propose MeshNet; it adopts graph-constrained mesh-cell nodes to integrate local-to-global geometric features. MeshNet [Feng et al. 2019] learns the spatial and structural features of a face by aggregating its 1-ring neighbors using two mesh convolutional layers. DNF-Net [Li et al. 2020] denoises mesh normals on cropped local patches using multi-scale embedding and a residual learning strategy. TextureNet [Huang et al. 2019] parameterizes mesh patches and high-resolution textures as quadrilaterals to employ grid convolution. However, extra effort must be made to remove singularities and directional ambiguity.

No regular and uniform hierarchy as subdivision is applied in the above methods. Except for Xu et al. [2017], other methods do not exploit distant neighbors of faces and thus have a limited perception field. Compared to Xu et al. [2017], our convolutions efficiently support stride and large dilation to better capture long-range features.

2.3 Subdivision Surfaces and Multiresolution Modeling

A subdivision surface is a smooth surface produced by refining a coarse mesh. The best-known mesh subdivision algorithms are Catmull-Clark subdivision [Catmull and Clark 1978] for quad meshes and Loop subdivision [Loop 1987] for triangle meshes. They insert new vertices and edges, split faces, and linearly update vertex positions. Other subdivision schemes, e.g. [Doo and Sabin 1978; Dyn
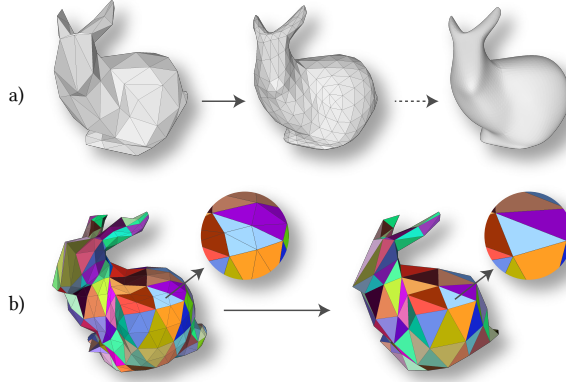
Fig. 2. a). Loop subdivision. A coarse mesh is iteratively refined by splitting each face into four and smoothing. b). The 4-to-1 face mapping from a fine mesh to the next coarser level using Loop subdivision sequence connectivity.

et al. 1990; Kobbelt 2000] and non-linear approaches, e.g. [Liu et al. 2006; Schaefer et al. 2008] have also been proposed.

Multi-resolution modeling, or level of detail, aims to construct a sequence of meshes from fine to coarse, and is widely applied in mesh compression, editing, and fast rendering. There are many works on this topic, and we merely consider methods that maintain a special subdivision sequence connectivity from fine to coarse. This is a key issue, as we need a whole hierarchy of meshes *all* having Loop subdivision connectivity. MAPS [Lee et al. 1998] is a pioneering work that computes a parameterization of a mesh over its simplified version. Then, a new mesh with subdivision sequence connectivity is constructed on the surface of the simplified mesh. Finally, the vertices of the new mesh are projected back to the surface of the input face via the parameterization. This idea is further improved in terms of distortion and smoothness by [Guskov et al. 2002, 2000; Khodakovsky et al. 2003; Kobbelt et al. 1999]. Liu et al [2020] have also extended the MAPS algorithm to generate multi-resolution meshes for network training.

Through a multi-resolution method, a mesh can be remeshed to be with subdivision sequence connectivity, making SubdivNet a general method for 3D mesh analysis.

3 SUBDIVNET

3.1 Preliminaries

Before we introduce the details of SubdivNet, we first explain the mathematical notations used throughout this paper.

A triangle mesh $\mathcal{M} = (V, F)$ is defined by a set of vertices $V = \{v_i | v_i \in \mathcal{R}^3\}$ and a set of triangular faces $F = \{f_i | f_i \in \{1, \cdots, |V|\}^3\}$, indicating the vertices of that triangle, and hence implicitly, the connectivity. Each face f_i holds an input feature vector e_i, which is to be processed by SubdivNet.

Two faces f_i and f_j are said to be adjacent if they share an edge. The distance $D(f_i, f_j)$ between f_i and f_j is defined as the minimum number of faces traversed by any path from one to the other across edges. Then, k-ring neighborhood of f_i is as follow:

$$\mathcal{N}_k(f_i) = \{f_j | D(f_i, f_j) = k\}.$$

We say that a triangle mesh $\mathcal{M}$ has *Loop subdivision connectivity* if it has the same topology as some mesh formed by one round of Loop subdivision acting on a coarser mesh.

We say that a triangle mesh $\mathcal{M}$ has *Loop subdivision sequence connectivity* if there exists a sequence of meshes $(\mathcal{M}_0, \cdots, \mathcal{M}_L)$, $d \geq 1$, where $\mathcal{M}_L = \mathcal{M}$, satisfying two requirements: (i) all except possibly $\mathcal{M}_0$ have Loop subdivision connectivity; (ii) all vertices in $\mathcal{V}_i$ are also present in $\mathcal{V}_{i+1}$, $0 < i < L$. The bunny in Fig. 1 shows an example of such a sequence.

We call L the *subdivision depth* of $\mathcal{M}$, $\mathcal{M}_0$ the *base mesh* of $\mathcal{M}$, and the number of faces of $\mathcal{M}_0$ is the *base size*. Clearly, the number of faces of $\mathcal{M}$ is $|F| = 4^L |F_0|$.

If $\mathcal{M}$ has Loop subdivision sequence connectivity, we can establish a 4-to-1 face mapping from each mesh $\mathcal{M}_i$, $i > 0$, to mesh $\mathcal{M}_{i-1}$, which can be regarded as the topological inverse of Loop subdivision ignoring vertex geometry updates (see Fig. 2(b)).

Most common meshes, whether designed by artists or scanned by sensors, lack Loop subdivision sequence connectivity. Hence, we first remesh the input mesh via a self-parameterization to give it this property, for a specified base size and subdivision depth, using methods explained in Sec. 4. In the rest of this section, we assume that the input mesh has already been remeshed appropriately.

3.2 Overview

Given a watertight 2-manifold triangle mesh with Loop subdivision sequence connectivity, this paper aims to learn a global representation for the 3D shape, or feature vectors on every face for local geometry.

Like a 2D image pyramid, $(\mathcal{M}_L, \cdots, \mathcal{M}_0)$ provides a hierarchical structure, or *mesh pyramid*. Through the 4-to-1 face mapping provided by Loop subdivision sequence connectivity, we can also establish an injection of faces from $\mathcal{M}_L$ to $\mathcal{M}_0$ step by step, allowing feature aggregation from local to global.

Based on this, SubdivNet takes a mini-batch of close 2-manifold triangle meshes with subdivision sequence connectivity as input. It computes features with convolutions defined on triangle faces, and aggregates long-range feature descriptions of meshes by uniform face downsampling. Similar to pooling on faces, our mesh convolutions are performed on faces. Because of the regular number of face neighbours, this mesh convolution also supports variable kernel size, dilation, and stride, acting like a standard convolution in the image domain. To support dense prediction tasks, e.g. segmentation, an upsampling operation is provided as the inverse of pooling.

Since this mesh convolution is flexible and general, we can directly adapt well-known networks from the 2D image domain to mesh learning tasks.

3.3 Convolution

In this section, we first talk about which faces should be taken into consideration in convolution, i.e. convolution kernel patterns Ω. Then we will describe how to perform the convolution with such kernels.

3.3.1 Basic Convolution Pattern. A key to defining convolution for a given signal is to specify its neighborhood, or kernel pattern. Since there are no boundary edges in a 2-manifold triangle mesh, each
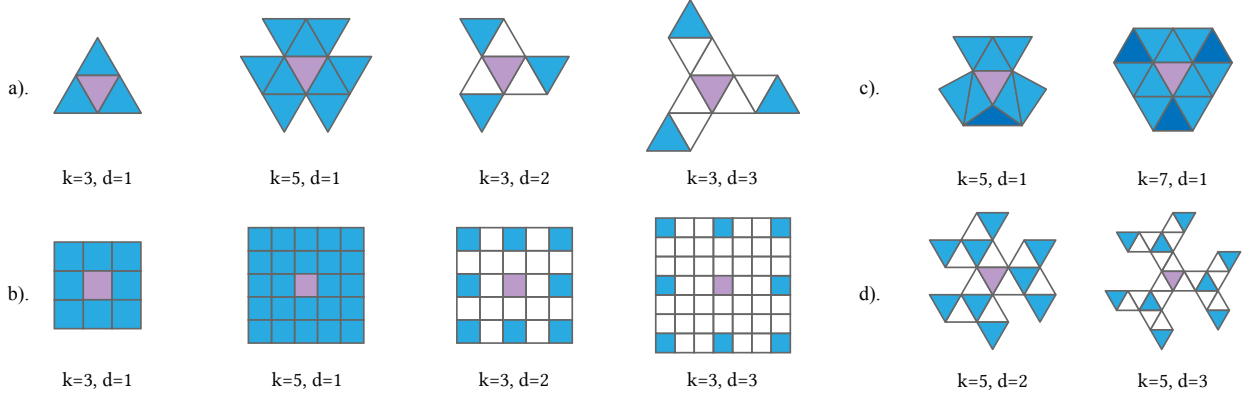
Fig. 3. Mesh convolution kernel pattern. (a) Mesh convolution kernels with different kernel size k and dilation d. (b) Corresponding 2D convolution kernels. (c) Duplication happens for kernel sizes larger than 3: deep blue faces are accessed twice. (d) More complex convolution kernels with larger kernel size and dilation.

face on the mesh has exactly 3 adjacent faces. This 3-regular property is analogous to the lattice connectivity of pixels in 2D images, motivating us to define a basic convolution over faces. Formally, for each face f_i, the basic convolution kernel pattern is its 1-ring neighbors $\Omega(f_i) = \mathcal{N}_1(f_i)$, illustrated in Fig 3(a).

3.3.2 Kernel Size. To permit an enlarged receptive field of the convolution, convolution in 2D images is designed to support a variable kernel size. This feature is also crucial in shape analysis to learn more discriminative representations for each vertex and face, facilitating tasks such as shape correspondence and segmentation. However, convolutions defined on meshes usually exploit a fixed kernel size. Instead, we consider additional nearby faces to define the pattern of a convolution with variable kernel size k, so

$$\Omega(f_i, k) = \bigcup_{i=1}^{\hat{k}} \mathcal{N}_{\hat{k}}(f_i), \quad \hat{k} = \frac{k-1}{2}, k = 1, 3, 5, \ldots \quad (1)$$

In total, there are $3 \times (2^{\hat{k}} - 1)$ faces in the kernel pattern with kernel size k. Fig. 3(a) illustrates a case with a kernel size of 5, for example.

However, when k is larger than 3, there may be adjacent faces that are counted more than once and the number of triangles in Ω is smaller than expected. Avoiding such issues would lead to a complex convolution design, so we simply retain all duplications of faces and keep the size of Ω fixed. Apart from simplicity, another reason is that a larger 2D convolution kernel is typically replaced by a stack of small kernels in modern network designs, typically no greater than size 5. When $k = 3$, there will not be duplication, and when $k = 5$, duplication can only exist around vertices whose degree is 4 or less (these vertices can only occur in the base mesh because of Loop subdivision sequence connectivity), see Fig. 3(c). When the kernel size is larger than 7, faces may be accessed more than twice.

3.3.3 Dilation. A popular variation of convolution is dilated convolution (or atrous convolution), where holes are inserted in the kernel pattern (see Fig 3(b)). Dilation is an efficient strategy for enlarging
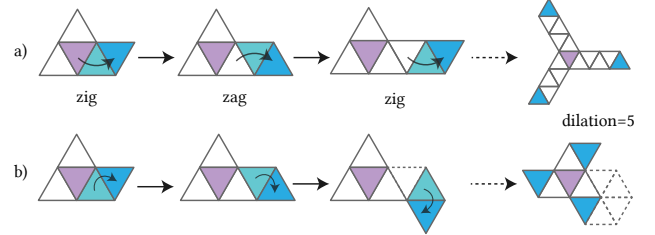

Fig. 4. (a) Zig-zag strategy provides a uniformly dilated convolution from the basic convolution pattern. (b) Alternative scheme folds back, causing the dilation pattern to select triangles too close to the central triangle.

the receptive field without increasing computational and memory resource requirements. To extend this concept to triangle meshes, we require that in a kernel pattern with dilation d, the distance between a face and its nearest face (including the center f_i) is d. Specially, the dilation of the basic convolution pattern is 1.

In a 2D image grid, the dilated kernel can be easily obtained by skipping rows and columns. However, such a strategy cannot be readily applied to triangle meshes due to the difference in connectivity (see Fig. 4(b)).

Instead, we propose a *zig-zag* strategy to define a kernel pattern with dilation d, shown in Fig 4(a). Taking a dilated convolution whose kernel size is 3 as an example, we move from faces in $\Omega(f_i, d)$ to neighbors in turn d times, alternately clockwise or counterclockwise with respect to the last position. Without loss of generality, if we assume that the input ordering of the three vertices in a face is counterclockwise, then 'zig' and 'zag' are counterclockwise and clockwise, respectively. Using the opposite definition is also possible, which leads to a different, but symmetric pattern.

For kernel sizes k larger than 3, theoretically, we may first find the k-ring neighbors and perform dilation before the finding $(k+1)$-ring neighbors (see Fig. 3(d)).

This is not the only way to define dilation, but this formulation is based on the face distance, consistent with what we do with

the kernel size. Another motivation is to ensure that $|\Omega(f_i, d)| = |\Omega(f_i, d = 1)|$ as required in 2D image grids. Also, the zig-zag style results in a uniform spatial distribution of elements in Ω, reducing the occurrence of duplicated faces.

One may notice that the proposed dilation is asymmetric. As a result, only elements from three directions are considered when kernel size is 3 while the information from the other three directions is lost, possibly leading to bias. However, with two or more dilated convolutions, features of all directions can be aggregated, and thus the potential bias is avoided.

3.3.4   Stride. In 2D CNNs, stride controls how densely the convolution is applied to the image. Since a 2D convolution with a stride larger than 1 reduces the resolution of the 2D feature map, it often is used for down-sampling, acting as a pooling layer with parameters.

Thus, we also define a strided convolution based on the mesh pyramid. When the mesh convolution has a stride, it is only applied to the central face of a group of adjacent faces mapping to the same face in the coarser mesh. Since 1-to-4 Loop subdivision is used throughout SubdivNet, the stride size is 2. To support an arbitrary stride size s, one can choose a 1-to-s^2 split subdivision scheme rather than the Loop subdivision scheme when remeshing the input. See Sec. 4 for further details.

3.3.5   Order-invariant Convolution Computation. The three neighbors of a face are unordered in the input, but a robust convolution should be initial ordering invariant. While $\Omega(f_i)$ is an unordered set, we can rearrange $\Omega(f_i)$ counterclockwise around f_i so that $\hat{\Omega}(f_i)$ is ordered as a closed ring to facilitate neighbor processing. Even so, where the ring ordering starts is still ambiguous, but we can utilize the property of a ring to remove the ambiguity. The rearrangement can be implemented by depth first search (DFS) when the kernel size > 3, the order of faces being determined by in-order traversal of the search tree. In our implementation, neighbor indexing is computed in parallel.

Inspired by MeshCNN [Hanocka et al. 2019], to further guarantee invariance to the input face order, we define the computation of convolution on a face f_i as,

$$\text{Conv}(f_i) = w_0 e_i + w_1 \sum_{j=1}^{n} e_j + w_2 \sum_{j=1}^{n} |e_{j+1} - e_j| + w_3 \sum_{j=1}^{n} |e_i - e_j|, \quad (2)$$

where $n = |\hat{\Omega}(f_i)|$, e_j is the feature vector on the jth face in $\hat{\Omega}(f_i)$ ($e_{n+1} = e_1$), and $w = (w_0, w_1, w_2, w_3)$ are learnable parameters. As $\hat{\Omega}(f_i)$ is a ring surrounding f_i, the sum of differences between e_{j+1} and e_j is ordering invariant.

3.4   Pooling

With the pyramid of input meshes, pooling on triangle meshes is as easy as on regular 2D image grids, as shown in Fig. 5: four subdivided faces in the finer mesh are pooled to the parent face in the coarser mesh.

Compared with the method in [Hanocka et al. 2019] that defines pooling via dynamic edge collapse, our approach is more simple, stable, and uniform. There, edge collapse must be implemented in sequence to maintain a half-edge data structure. The collapse order is specified by a pre-defined priority and non-manifoldness has to
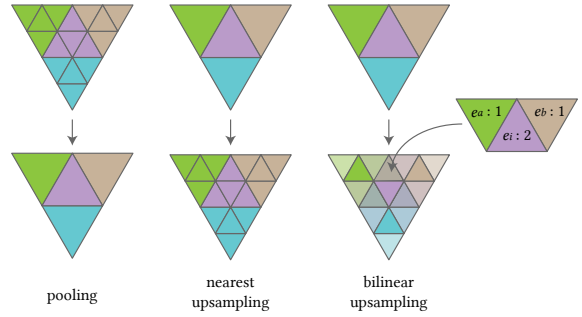

Fig. 5.   Pooling and upsampling

be avoided. Such edge pooling cannot guarantee uniform pooling. On the other hand, our pooling approach can be implemented in parallel, and subdivision connectivity guarantees that every 4 faces are uniformly pooled to 1.

Like the convolution stride, the pooling operation supports a stride s larger than 2 via a 1-to-s^2 subdivision scheme when preprocessing the input meshes.

3.5   Upsampling

As the reverse of pooling, upsampling is also defined with the help of the mesh pyramid. A *nearest upsampling* operation simply splits a face into 4 faces; features on split faces are copied from the original face, as in Fig. 5.

In 2D dense prediction tasks, bilinear upsampling is also widely used. Therefore, we also define a *bilinear upsampling* operation based on face distance, to provide a smoother interpolation than the nearest upsampling. See Fig. 5. The feature of the central subdivided face f_i is set equal to the original face's feature, and features of the other faces f_j are computed by

$$e_j = \frac{1}{2} e_i + \frac{1}{4} e_a + \frac{1}{4} e_b, \quad (3)$$

where f_a and f_b are the other two faces adjacent to f_j.

3.6   Network Architecture

We now show how the novel mesh convolution defined above can be integrated within deep neural networks for general tasks such as mesh classification and segmentation.

For classification, we simply use two blocks of basic convolution, batch normalization, and ReLU layers at each resolution. Max-pooling is utilized for down-sampling. Experimentally, we find this simple convolutional network achieves sufficient performance due to the representational power of our mesh convolution.

When we apply the simple network to segmentation, the benefits to accuracy are not as significant as for the classification task. Therefore, we employ a more carefully designed network architecture for this dense prediction task.

Deeplab v3+ [Chen et al. 2018] is a 2D segmentation network providing state-of-the-art performance. Its key idea is to use dilated convolutions to enlarge the perceptive field. Because of the flexibility of our mesh convolution, we can easily adapt its architecture to 3D mesh tasks. Since the raw training data meshes (before remeshing)
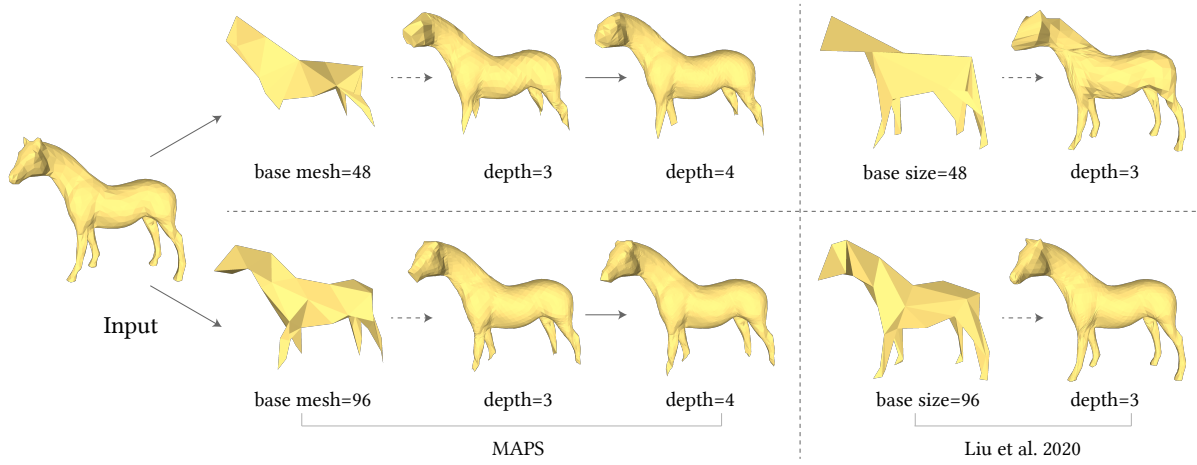
Fig. 6. Comparison of remeshing results of MAPS and Liu et al. [2020]. MAPS first decimates the input mesh, and constructs a bijection between the original mesh and the base mesh. Then the base mesh is subdivided and new vertices are projected back onto the input. Limited sampling in the base mesh leads to obvious distortion, e.g. in the limbs. Liu et al.'s approach produces remeshing results of higher quality.

typically have far fewer triangles than pixels in a 2D image, we simply use ResNet50 [He et al. 2016] as a feature extractor instead of xception [Chollet 2017] both for efficiency and to avoid overfitting. Again because of the smaller number of triangles, we also reduce the number of downsampling layers to 3. Convolutions with different kernel size, stride, and dilation are all employed in Deeplab v3+; we can also provide all of them in our mesh version. Following Deeplab v3+, we use two bilinear upsampling layers to create a 4×4 upsampling layer in the decoder of the original network.

3.7 Input features

The input feature for each triangle face is a 13-dimensional vector, which is divided into a 7-dimensional shape descriptor and a 6-dimensional pose descriptor. The components of the shape descriptor are the face area, the three interior angles of the triangle, and the inner products of the face normal with the three vertex normals (the last term characterizing curvature). The pose descriptor is the position of the face center and the face normal, helping the network to identify faces with similar shapes through position and orientation. Further user-defined features such as colors may also be added for specific learning tasks.

4 REMESHING FOR SUBDIVISION CONNECTIVITY

SubdivNet requires meshes with Loop subdivision sequence connectivity as input; however, most available meshes do not have this property. We thus must remesh any input mesh to have this property beforehand.

One solution is to use a self-parameterization method, e.g. , the MAPS algorithm [Lee et al. 1998] and the modified version [Liu et al. 2020]. The key idea is to establish a mapping between an input mesh and its simplified mesh, i.e. the base mesh. Thus, by subdividing the base mesh and a back-projection on the input mesh, we can remesh the input with subdivision sequence connectivity. Sometimes, the output of MAPS has obvious distorted details. Liu et al. improve the
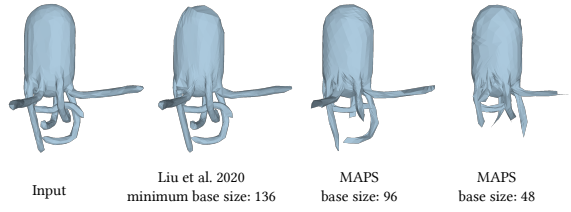

Fig. 7. An octopus mesh from the SHREC11 dataset [Wang et al. 2012]. Liu et al.'s [2020] method cannot produce a lower base mesh size than 136 triangles. However, MAPS can reduce the base size while keeping important features. For example, although shortened, the number of tentacles is unchanged. The subdivision depth in each case is 3.

quality of output but cannot reach a low base size when the input mesh is complicated (see Fig. 7). Please refer to App. A for more details.

In practice, we adopt a simple strategy to switch remeshing approaches based on different tasks. For tasks where the overall shape is more important and distortion can be tolerated, e.g. classification, we choose the MAPS algorithm to achieve a greater degree of global feature aggregation, while for tasks where local details are more crucial, e.g. fine-grained segmentation, we use Liu et al.'s approach and use a relatively larger base size.

Specifically, for the classification task, the base mesh size is 48, similar to the 7×7 feature map in ResNet [He et al. 2016]. The subdivision depth is set to 4, leading to 12288 faces in the finest mesh. For dense prediction tasks, the base mesh size and subdivision depth are 256 and 3, respectively, to balance the prediction quality and computational efficiency. We find these hyper-parameters work well for evaluation on public datasets. But for meshes with higher resolution, one may choose a larger subdivision depth for better results.

Both MAPS and Liu et al. [2020] require the input meshes to be manifold and closed, otherwise the local parameterizations may fail. Other meshes must be converted to watertight manifolds beforehand, via additional preprocessing (see App. B).

5 EXPERIMENTS

The generality and flexibility of our mesh convolution permit SubdivNet to be applied to a wide range of 3D shape analysis tasks. We have quantitatively evaluated SubdivNet for mesh classification, mesh segmentation, and shape correspondence, comparing it to other state-of-the-art alternatives. We have conducted other qualitative experiments to demonstrate its applicability in other areas such as real-world mesh retrieval. Key components of SubdivNet are also evaluated for effectiveness.

5.0.1 Data preprocessing and augmentation. As the meshes in the datasets do not have Loop subdivision sequence connectivity, we first remesh all data from both training and test sets. As described in Sec. 4, the remeshing methods are able to produce multiple remeshed results by randomizing vertex removal order. Considering that some datasets are small, multiple remeshed meshes for each input were generated by randomly permuting the order of vertices when they are presented for remeshing. The augmentation helps the network to be insensitive to remeshing.

To make the network less sensitive to shape scale, we first scale the input to fit inside a unit cube and apply random anisotropic scaling with a normal distribution $\mu = 1$ and $\sigma = 0.1$, following [Hanocka et al. 2019]: for example, some human body shapes are taller but thinner than others. We also notice that some orientations of shapes in the test dataset do not appear in the training dataset, e.g. in the human body dataset [Maron et al. 2017]. Therefore, for such datasets, we also randomly changed the orientation of the input data by rotating around the three axes with Euler angles of 0, $\pi/2$, π, or $3\pi/2$.

5.1 Classification

We first demonstrate the power of SubdivNet on the mesh classification task with three datasets. As for the data augmentation adopted during training, we also generate 10 to 20 remeshed meshes for each mesh in the test, and a majority voting strategy is applied to reduce the variance introduced by remeshing.

5.1.1 SHREC11. The SHREC11 dataset [Wang et al. 2012], which contains 30 subjects with 20 samples in each class. Following the setting in [Hanocka et al. 2019], SubdivNet is evaluated on two protocols where there are 16 or 10 training examples in each class. We report the average accuracy on 3 random splits into training and test set in Table 1. SubdivNet correctly classifies all test meshes. Even without majority voting, SubdivNet is still comparable to or outperforms other state-of-the-art methods. In fact, using voting, accuracy already reaches 100% when accuracy without voting is around 95% in training. This suggests that the proposed method is accurate enough for the SHREC11 mesh classification task.

5.1.2 Cube Engraving. The Cube Engraving dataset [Hanocka et al. 2019] was synthesized by engraving 2D shapes on one random face of a cube. There are 22 categories and 4,381 shapes in the publicly

Table 1. Classification accuracy on the SHREC11 datset [Wang et al. 2012]

Method	Split 16	Split 10
GWCNN [Ezuz et al. 2017]	96.6%	90.3%
MeshCNN [Hanocka et al. 2019]	98.6%	91.0%
PD-MeshNet [Milano et al. 2020]	99.7%	99.1%
MeshWalker [Lahav and Tal 2020]	98.6%	97.1%
SubdivNet (w/o majority voting)	**99.9**%	**99.5**%
SubdivNet	**100**%	**100**%

Table 2. Classification accuracy on the Cube Engraving dataset [Hanocka et al. 2019].

Method	Accuracy
PointNet++ [Qi et al. 2017b]	64.3%
MeshCNN [Hanocka et al. 2019]	92.2%
PD-MeshNet [Milano et al. 2020]	94.4%
MeshWalker [Lahav and Tal 2020]	98.6%
SubdivNet (w/o majority voting)	**98.9**%
SubdivNet	**100.0**%

Table 3. Classification accuracy on ModelNet40 [Wu et al. 2015] and Manifold40. The first two rows are state-of-the-art point cloud methods with positions and normals as input. Other methods input meshes.

Method	ModelNet40	Manifold40
PointNet++ [Qi et al. 2017a]	91.7%	87.9%
PCT [Guo et al. 2021]	93.2%	**92.4**%
SNGC [Haim et al. 2019]	91.6%	-
MeshNet [Feng et al. 2019]	91.9%	88.4%
MeshWalker [Lahav and Tal 2020]	92.3%	90.5%
SubdivNet	-	**91.4**%

released dataset. Table 2 shows that SubdivNet is the first method to reach zero classification errors.

5.1.3 Manifold40. ModelNet40 [Wu et al. 2015], containing 12,311 shapes in 40 categories, is a widely used benchmark for 3D geometry learning. However, most 3D shapes in ModelNet40 are not watertight or 2-manifold, leading to remeshing failures. Therefore, we reconstructed the shapes in ModelNet40 and built a corresponding *Manifold40* dataset, in which all shapes are closed manifolds. See App. B for details of Manifold40 and the particular experimental settings used.

We trained and evaluated point cloud methods, MeshNet [Feng et al. 2019], MeshWalker [Lahav and Tal 2020], and SubdivNet on Manifold40; results are shown in Table 3. Because of the reconstruction error and simplification distortion, Manifold40 is more challenging and the accuracy of all other methods tested drops. SubdivNet again outperforms all mesh-based methods on Manifold40.

5.2 Segmentation

For the mesh segmentation task, SubdivNet is trained to predict labels for every face. Due to the process of remeshing, the remeshed faces should be appropriately labeled before we can start training.

Table 4. Mesh segmentation accuracy on the human body dataset [Maron et al. 2017]

Method	Accuracy
Pointnet [Qi et al. 2017a]	74.7%
Pointnet++ [Qi et al. 2017b]	82.3%
Toric Cover [Maron et al. 2017]	88.0%
MeshCNN [Hanocka et al. 2019]	87.7%
MeshCNN (10000 faces)	65.3%
PD-MeshNet [Milano et al. 2020]	86.9%
SNGC [Haim et al. 2019]	91.3%
MeshWalerk [Lahav and Tal 2020]	92.7%
SubdivNet (w/o majority voting)	91.1%
SubdivNet	**93.0**%

To do so, we simply adopt a nearest-face strategy to build a mapping between the raw mesh and the remeshed one. In the test stage, the predicted labels of the raw mesh are also determined in this way.

Another issue is the lack of an agreed evaluation metric. Both PD-MeshNet [Milano et al. 2020] and MeshCNN [Hanocka et al. 2019] are evaluated over simplified meshes, and MeshCNN reports the accuracy on edges. For a fair comparison, we project their predictions back to the raw meshes as well. Specifically, to transfer the results of MeshCNN to faces in the raw mesh, we first find the nearest triangle to its face center in the simplified mesh, and take the label of the nearest edge in the triangle as the prediction. For point cloud methods [Qi et al. 2017a,b], we uniformly sample 4096 points on the mesh surface, and also use the nearest strategy to compute accuracy for the raw mesh. The result using MeshCNN's metric is reported in App. C for comparison.

5.2.1 Human Body Segmentation. The human body dataset, labeled by [Maron et al. 2017], contains 381 training shapes from SCAPE [Anguelov et al. 2005], FAUST [Bogo et al. 2014], MIT [Vlasic et al. 2008], Adobe Fuse [Adobe.com 2021], and 18 test shapes from SHREC07 [Giorgi et al. 2007]. The human bodies are segmented into 8 parts. Here we used Liu et al.'s method [Liu et al. 2020] to remesh the inputs to ensure lower distortion of details. The majority voting is also employed in the test stage. Results are listed in Table 4, showing that our proposed method also outperforms other methods.

The input resolution of MeshCNN [Hanocka et al. 2019] is 1,500 faces. To find out whether the performance of MeshCNN is influenced by the resolution, we additionally train MeshCNN with 10,000 faces for a fair comparison. The dramatical decline in accuracy suggests that the increase of performance does not come from the higher resolution, but the delicate design.

Some examples of the segmentation results are visualized in Fig. 8. Compared to MeshCNN [Hanocka et al. 2019] and PD-MeshNet [Milano et al. 2020], SubdivNet generates more accurate part segmentation, as well as more consistent boundaries, benefitting from our generic and flexible mesh convolution.

5.2.2 COSEG. We also evaluated SubdivNet on the three largest sets from the COSEG shape dataset [Wang et al. 2012]: tele-aliens, chairs, and vases, with 200, 400, and 300 models, respectively. They are labeled into only 3 or 4 parts, so we choose the MAPS algorithm
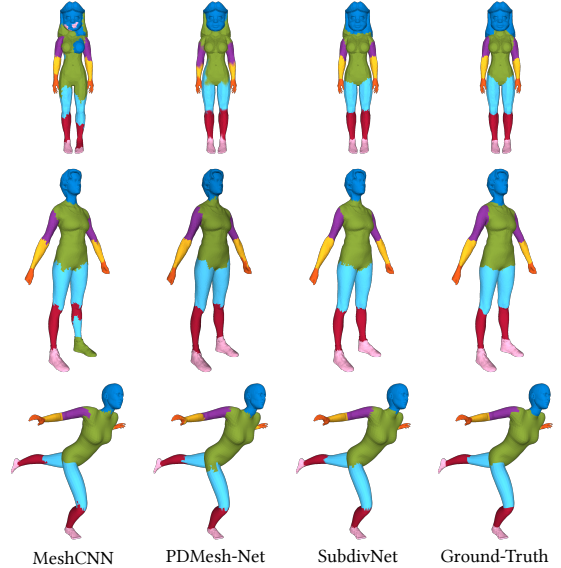

Fig. 8. Segmentation results from the human body dataset [Maron et al. 2017]. SubdivNet correctly classified all body parts, and gave more accurate boundaries.

Table 5. Mesh segmentation accuracy on the COSEG dataset [Wang et al. 2012].

Method	Vases	Chairs	Tele-aliens
DCN [Xu et al. 2017]	90.9%	95.7%	-
MeshCNN [Hanocka et al. 2019]	85.2%	92.8%	94.4%
PD-MeshNet [Milano et al. 2020]	81.6%	90.0%	89.0%
SubdivNet	**96.7**%	**96.7**%	**97.3**%

as the remeshing method. We randomly split the training set and test set with a ratio of 4:1. Then, SubdivNet is trained on the three datasets separately. Quantitative results are provided in Table 5 and example results are displayed in Fig. 9. Our method also achieves significant improvement over MeshCNN [Hanocka et al. 2019] and PD-MeshNet [Milano et al. 2020].

5.3 Shape Correspondence

Our method can act as a robust feature extraction backbone for learning fine-grained shape correspondences from two meshes. We demonstrate this by the task of human body matching using FAUST [Bogo et al. 2014] and SCAPE [Anguelov et al. 2005] dataset. Specifically, our network is trained to predict 3-dimensional canonical human coordinates similar to [Mehta et al. 2017] but on the mesh level. The set of predicted coordinates is treated as an $\mathcal{R}^3$-valued function and the functional coordinates (dimension = 30) are computed based on the spectrum of the Laplace-Beltrami operator on the corresponding mesh. We then build a functional map, a representation for non-rigid shape matching, between the source and target meshes by solving a linear system as in [Ovsjanikov et al. 2012]. Lastly, the map is refined using ZoomOut [Melzi et al. 2019] and converted back into point-to-point correspondence. Note
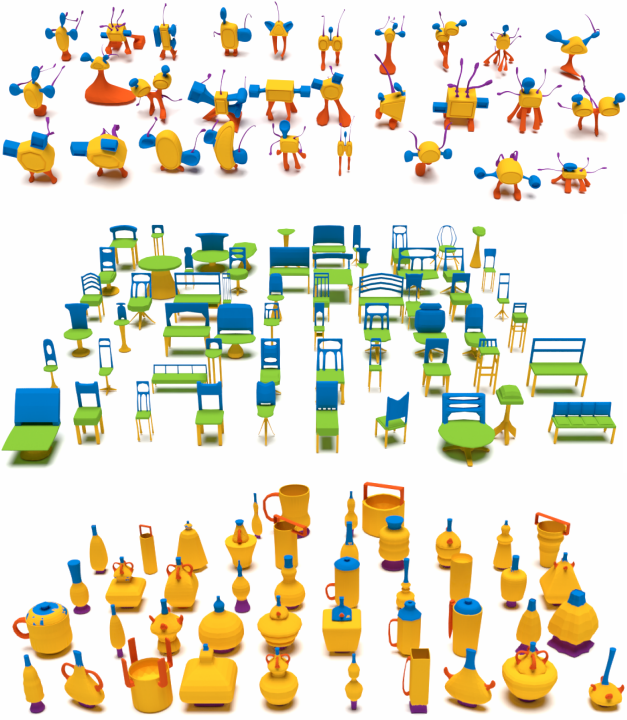
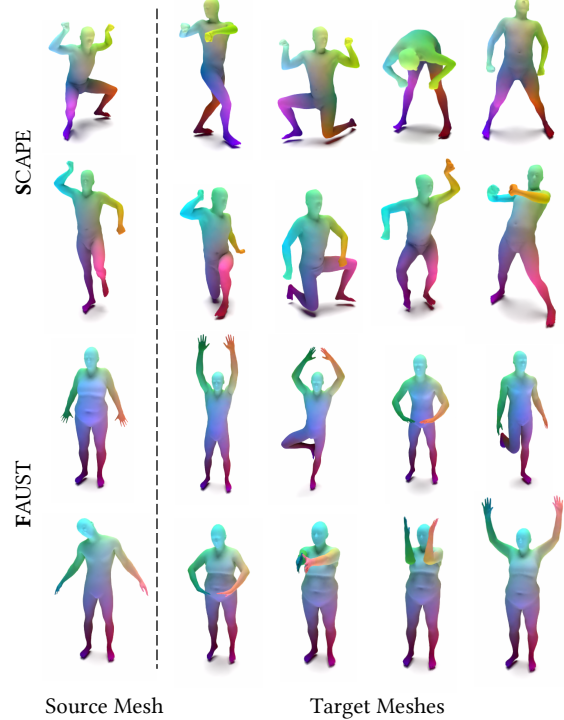Fig. 9. Gallery of segmentation results for the COSEG dataset.

Fig. 10. The learned shape correspondences on different datasets using our method. Each row shows the matching results from the source mesh to the target meshes on the right. Note how corresponding positions share the same color.

that due to the small amount of data, we additionally remesh our geometries with different subdivision connectivities as augmentation during network training, which enforces the model to learn a tessellation-invariant robust feature.

Our evaluation protocol follows Bogo et al. [2014] and Donati et al. [2020]: The shape correspondence error is calculated as the normalized mean geodesic distance between predicted and ground-truth mapped target positions on the target mesh. The datasets, namely FAUST and SCAPE, are respectively divided into 80:20 and 51:20 training/test splits. Results from different combinations of the training and test sets are reported in Table 6 and visualized in Fig. 10. Our method achieves state-of-the-art matching results and shows good generalizability across different datasets, demonstrating the effectiveness of the proposed method on this challenging task.

5.4 Further Evaluation

5.4.1 Network Architecture. To illustrate that well-known network architectures for 2D images can be directly applied to 3D meshes using our convolution and pooling methods, we evaluate a naive U-Net [Ronneberger et al. 2015] in addition to Deeplab v3+ [Chen et al. 2018] for the task of segmentation. The U-Net only consists of basic convolutions, with skip-connections are added between the encoder and the decoder. Table 7 indicates that network architecture transfer is effective. The results are unsurprising because we treat the faces as the basic unit of a 3D shape. The similarity between faces and pixels leads to the same problems that U-Net faces. For instance,

Table 6. Shape correspondence error (×100) comparison. 'F' and 'S' means FAUST [Bogo et al. 2014] and SCAPE [Anguelov et al. 2005] dataset. 'F on S' means training on FAUST and testing on SCAPE and vice versa.

Method	F	S	F on S	S on F
BCICP [Ren et al. 2018]	15.	16.	-	-
ZoomOut [Melzi et al. 2019]	6.1	7.5	-	-
SURFMNet [Roufosse et al. 2019]	7.4	6.1	19.	23.
FMNet [Litany et al. 2017]	5.9	6.3	11.	14.
3D-CODED [Groueix et al. 2018]	2.5	31.	31.	33.
GeomFMaps [Donati et al. 2020]	**1.9**	**3.0**	9.2	4.3
Ours	**1.9**	**3.0**	10.5	**2.6**

Table 7. Segmentation results for different network architectures on the human body dataset [Maron et al. 2017].

Network Architecture	Accuracy
U-Net [Ronneberger et al. 2015]	89.5%
Deeplab v3+ [Chen et al. 2018]	93.0%

since there is no dilation in U-Net, it suffers from the limited size of the perceptive field.

5.4.2 Input features. Unlike image pixels, whose shape is identical everywhere, the shapes of mesh triangle faces represent the local

Table 8. Ablation study of input features on Human Body Segmentation [Maron et al. 2017]. The backbone used is DeepLabV3+.

Input	Accuracy
only shape descriptor	90.4%
only pose descriptor	92.5%
full input	93.0%

Table 9. Classification accuracy on the SHREC11 (split 10) [Wang et al. 2012] with different input size.

Base Size	Subdivision Depth	Accuracy
48	3	99.3%
96	3	99.1%
48	4	99.4%

Table 10. Computation time and GPU memory consumption of SubdivNet, MeshCNN [Hanocka et al. 2019], and the 2D Deeplab v3+ [Chen et al. 2018]. The number of layers of 2D Deeplab v3+ is reduced to be the same as SubdivNet. Numbers are averaged over 1000 data samples.

Network	Input Size (faces/pixels)	Time (ms)	GPU Memory (MB)
SubdivNet (Deeplab v3+)	16384	47.4	1221
MeshCNN	10000	1051.2	4090
2D Deeplab v3+	16384	20.1	612

geometry. Thus, shape descriptors of the input features, i.e. areas, angles, and curvatures, are essential to the capability of SubdivNet. Table 8 indicates that both shape and pose are necessary for mesh learning.

5.4.3 Input Resolution. To examine the robustness of our network to input size, we try different combinations of the base size and subdivision depth of inputs and retrain the network on *Split10*. Table 9 suggests that performance varies little. Because the remeshing distortion is more observable as the input size decreases, the results also show that our network can capture the global shape and is robust to input distortion.

5.4.4 Computation Time and Memory Consumption. Our method is implemented with Jittor deep learning framework [Hu et al. 2020]. Its flexibility enables efficient face neighbor indexing; convolution can be implemented with general matrix multiplication operators. This allows the proposed network is to be as efficient as 2D networks.

We record times for forward and backward propagation and GPU memory consumption. Table 10 shows that SubdivNet is more than 20× faster than an edge-based approach [Hanocka et al. 2019] with less than a third of GPU memory consumption, achieving comparable performance to a highly optimized 2D CNN [Chen et al. 2018].

5.5 3D shape retrieval from the real-world

The superior representation power of SubdivNet allows us to effectively extract global shape descriptors for arbitrary 3D meshes. We
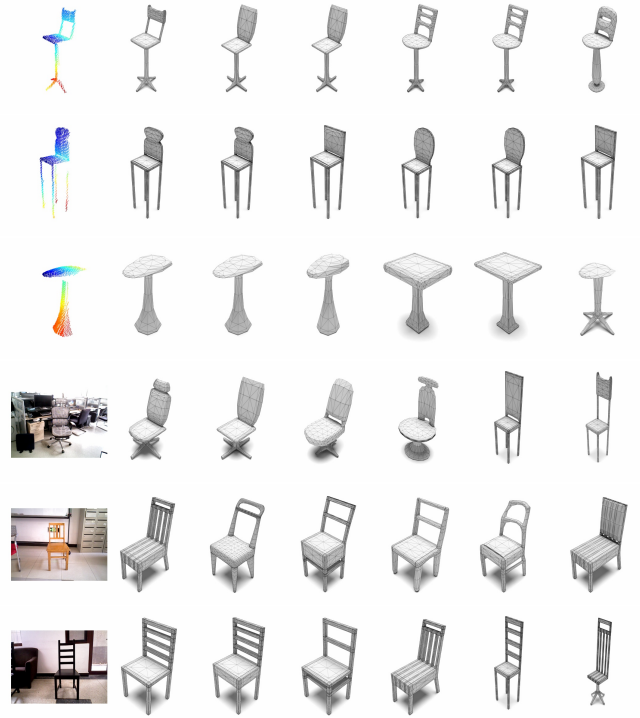

Fig. 11. Shape retrieval results using our method. The first column of each row shows input point clouds and other columns list retrieved results. The last three rows are from real-world RGB-D captures, where only the back-projected depth points are taken as input. Retrieval results are ordered from left to right by similarity in feature space.

demonstrate this using the task of 3D shape retrieval from partially-observed point clouds captured by an Asus Xtion Pro Live 3D sensor. By jointly embedding both point clouds and meshes into the latent feature space, shape retrieval can be implemented as nearest neighbor search in the Euclidean-structured latent manifold. Specifically, to build such a latent space, we first train a denoising point cloud variational auto-encoder using the encoder architecture from [Qi et al. 2017a] and the decoder network from [Fan et al. 2017]. The point clouds are synthesized from the mesh dataset with virtual cameras. Then we extract the bottleneck features (dimension = 32) corresponding to all point clouds in our dataset and use them to directly supervise SubdivNet, obtaining a mapping from the mesh space to the latent space.

We train our network using the chair models from the COSEG dataset [Wang et al. 2012]. The evaluation on the synthetic point clouds gives top1, top5, and top10 recall rates of 76.8%, 83.3%, and 88.0%, respectively. Fig. 11 shows retrieval results for both synthetic point clouds and real-world depth scans.

6 LIMITATIONS AND FUTURE WORK

6.1 Convolution

In this work, we have designed a series of convolution kernel patterns over mesh faces by analogy with 2D convolutions, providing an effective basis for 3D geometry learning.

Like any analogy, past some point it breaks down. Convolutions in 2D CNNs have their origins in signal filtering. In our framework, we must take care to ensure that the convolution is ordering-invariant, so we first transform the neighborhood features, rather than apply direct signal convolutions. One consequence is that the number of convolution parameters does not increase with kernel size as for 2D convolutions. One possible strategy is to differentiate faces by their distances to the center. Even though the current formulation has worked well in our experiments, further exploration is needed to relate mesh convolution operations and their effectiveness.

6.2 Subdivision Connectivity

Subdivision connectivity plays a crucial role in SubdivNet, providing a uniform feature aggregation scheme from local to global. We believe it is a key factor in our method surpassing other mesh learning methods.

However, remeshing is necessary to apply our method to an arbitrary mesh. As discussed in Sec. 4, both remeshing approaches we have used have limitations, with a trade-off between mesh quality and base mesh size. Further considerations are needed for how best to process imperfect meshes, polygon soups, shapes with boundaries, and large-scale scenes that usually have faults. We also note that majority voting improves the final performance, highlighting that the differences between the remeshed shape and the raw mesh affect the results to some extent. Better methods of remeshing [Sharp et al. 2019] are needed, or best of all, ways of downsampling without needing remeshing at all.

6.3 Applications

Apart from the applications in the paper, our ideas could potentially be applied to traditional geometric problems, such as mesh smoothing and denoising, deformation, registration of multiple meshes, etc. They could also be applied in specific areas that require human knowledge or professional skills. For example, we could learn the natural right way up for a mesh, or to choose the best orientation of a mesh for 3D printing [Ezair et al. 2015].

7 CONCLUSIONS

This work has presented a novel deep learning framework, SubdivNet, for 3D geometry learning on meshes. The core of SubdivNet is a general and flexible mesh convolution using a mesh pyramid structure for effective feature aggregation. We first utilize self-parameterization to remesh the input mesh to have Loop subdivision sequence connectivity. That allows a well-defined, uniform mesh hierarchy to be constructed over the input shape. We then use mesh convolution operators which support user-specified kernel size, stride, and dilation. Pooling and upsampling are also naturally supported by the subdivision connectivity. This enables the direct application of well-known 2D image CNNs to mesh learning.

Our evaluations indicate that SubdivNet surpasses existing mesh learning approaches in both accuracy and efficiency.

REFERENCES

Adobe.com. 2021. *Animate 3D characters for games, film, and more.* Retrieved Janurary 24, 2021 from https://www.mixamo.com

Dragomir Anguelov, Praveen Srinivasan, Daphne Koller, Sebastian Thrun, Jim Rodgers, and James Davis. 2005. SCAPE: shape completion and animation of people. *ACM Trans. Graph.* 24, 3 (2005), 408–416.

Federica Bogo, Javier Romero, Matthew Loper, and Michael J. Black. 2014. FAUST: Dataset and Evaluation for 3D Mesh Registration. In *CVPR*. IEEE Computer Society, 3794–3801.

Davide Boscaini, Jonathan Masci, Emanuele Rodolà, and Michael M. Bronstein. 2016. Learning shape correspondence with anisotropic convolutional neural networks. In *NIPS*. 3189–3197.

Michael M. Bronstein, Joan Bruna, Yann LeCun, Arthur Szlam, and Pierre Vandergheynst. 2017. Geometric Deep Learning: Going beyond Euclidean data. *IEEE Signal Process. Mag.* 34, 4 (2017), 18–42.

E. Catmull and J. Clark. 1978. Recursively generated B-spline surfaces on arbitrary topological meshes. *Computer-Aided Design* 10, 6 (1978), 350–355.

Liang-Chieh Chen, Yukun Zhu, George Papandreou, Florian Schroff, and Hartwig Adam. 2018. Encoder-Decoder with Atrous Separable Convolution for Semantic Image Segmentation. In *ECCV (7) (Lecture Notes in Computer Science)*, Vol. 11211. Springer, 833–851.

Y. Chen, J. Zhao, C. Shi, and D. Yuan. 2020. Mesh Convolution: A Novel Feature Extraction Method for 3D Nonrigid Object Classification. *IEEE Transactions on Multimedia* (2020), 1–1. https://doi.org/10.1109/TMM.2020.3020693

François Chollet. 2017. Xception: Deep Learning with Depthwise Separable Convolutions. In *CVPR*. IEEE Computer Society, 1800–1807.

Paolo Cignoni, Marco Callieri, Massimiliano Corsini, Matteo Dellepiane, Fabio Ganovelli, and Guido Ranzuglia. 2008. MeshLab: an Open-Source Mesh Processing Tool. In *Eurographics Italian Chapter Conference*. Eurographics, 129–136.

Nicolas Donati, Abhishek Sharma, and Maks Ovsjanikov. 2020. Deep Geometric Functional Maps: Robust Feature Learning for Shape Correspondence. In *CVPR*. IEEE, 8589–8598.

Daniel Doo and Malcolm Sabin. 1978. Behaviour of recursive division surfaces near extraordinary points. *Computer-Aided Design* 10, 6 (1978), 356–360.

Nira Dyn, David Levine, and John A. Gregory. 1990. A butterfly subdivision scheme for surface interpolation with tension control. *ACM Trans. Graph.* 9, 2 (1990), 160–169.

Ben Ezair, Fady Massarwi, and Gershon Elber. 2015. Orientation analysis of 3D objects toward minimal support volume in 3D-printing. *Comput. Graph.* 51 (2015), 117–124.

Danielle Ezuz, Justin Solomon, Vladimir G. Kim, and Mirela Ben-Chen. 2017. GWCNN: A Metric Alignment Layer for Deep Shape Analysis. *Comput. Graph. Forum* 36, 5 (2017), 49–57.

Haoqiang Fan, Hao Su, and Leonidas J Guibas. 2017. A point set generation network for 3d object reconstruction from a single image. In *Proceedings of the IEEE conference on computer vision and pattern recognition*. 605–613.

Yutong Feng, Yifan Feng, Haoxuan You, Xibin Zhao, and Yue Gao. 2019. MeshNet: Mesh Neural Network for 3D Shape Representation. In *AAAI*. AAAI Press, 8279–8286.

Michael Garland and Paul S. Heckbert. 1997. Surface simplification using quadric error metrics. In *SIGGRAPH*. ACM, 209–216.

Daniela Giorgi, Silvia Biasotti, and Laura Paraboschi. 2007. Shape retrieval contest 2007: Watertight models track. *SHREC competition* 8, 7 (2007).

Shunwang Gong, Lei Chen, Michael M. Bronstein, and Stefanos Zafeiriou. 2019. Spiral-Net++: A Fast and Highly Efficient Mesh Convolution Operator. In *ICCV Workshops*. IEEE, 4141–4148.

Thibault Groueix, Matthew Fisher, Vladimir G. Kim, Bryan C. Russell, and Mathieu Aubry. 2018. 3D-CODED: 3D Correspondences by Deep Deformation. In *ECCV (2) (Lecture Notes in Computer Science)*, Vol. 11206. Springer, 235–251.

Meng-Hao Guo, Jun-Xiong Cai, Zheng-Ning Liu, Taijiang Mu, Ralph R. Martin, and Shi-Min Hu. 2021. PCT: Point cloud transformer. *Comput. Vis. Media* (2021).

Igor Guskov, Andrei Khodakovsky, Peter Schröder, and Wim Sweldens. 2002. Hybrid meshes: multiresolution using regular and irregular refinement. In *Symposium on Computational Geometry*. ACM, 264–272.

Igor Guskov, Kiril Vidimce, Wim Sweldens, and Peter Schröder. 2000. Normal meshes. In *SIGGRAPH*. ACM, 95–102.

Niv Haim, Nimrod Segol, Heli Ben-Hamu, Haggai Maron, and Yaron Lipman. 2019. Surface Networks via General Covers. In *ICCV*. IEEE, 632–641.

Rana Hanocka, Amir Hertz, Noa Fish, Raja Giryes, Shachar Fleishman, and Daniel Cohen-Or. 2019. MeshCNN: a network with an edge. *ACM Trans. Graph.* 38, 4 (2019), 90:1–90:12.

Kaiming He, Xiangyu Zhang, Shaoqing Ren, and Jian Sun. 2016. Deep Residual Learning for Image Recognition. In *CVPR*. IEEE Computer Society, 770–778.

Sepp Hochreiter and Jürgen Schmidhuber. 1997. Long Short-Term Memory. *Neural Comput.* 9, 8 (1997), 1735–1780.

Shi-Min Hu, Dun Liang, Guo-Ye Yang, Guo-Wei Yang, and Wen-Yang Zhou. 2020. Jittor: a novel deep learning framework with meta-operators and unified graph execution. *Science China Information Sciences* 63, 12 (2020), 222103:1–222103:21.

Jingwei Huang, Hao Su, and Leonidas J. Guibas. 2018. Robust Watertight Manifold Surface Generation Method for ShapeNet Models. *CoRR* abs/1802.01698 (2018).

Jingwei Huang, Haotian Zhang, Li Yi, Thomas A. Funkhouser, Matthias Nießner, and Leonidas J. Guibas. 2019. TextureNet: Consistent Local Parametrizations for Learning From High-Resolution Signals on Meshes. In *CVPR*. Computer Vision Foundation / IEEE, 4440–4449.

Andrei Khodakovsky, Nathan Litke, and Peter Schröder. 2003. Globally smooth parameterizations with low distortion. *ACM Trans. Graph.* 22, 3 (2003), 350–357.

Roman Klokov and Victor S. Lempitsky. 2017. Escape from Cells: Deep Kd-Networks for the Recognition of 3D Point Cloud Models. In *ICCV*. IEEE Computer Society, 863–872.

Leif Kobbelt. 2000. 3-subdivision. In *SIGGRAPH*. ACM, 103–112.

Leif Kobbelt, Jens Vorsatz, Ulf Labsik, and Hans-Peter Seidel. 1999. A Shrink Wrapping Approach to Remeshing Polygonal Surfaces. *Comput. Graph. Forum* 18, 3 (1999), 119–130.

Ilya Kostrikov, Zhongshi Jiang, Daniele Panozzo, Denis Zorin, and Joan Bruna. 2018. Surface Networks. In *CVPR*. IEEE Computer Society, 2540–2548.

Alon Lahav and Ayellet Tal. 2020. MeshWalker: deep mesh understanding by random walks. *ACM Trans. Graph.* 39, 6 (2020), 263:1–263:13.

Aaron W. F. Lee, Wim Sweldens, Peter Schröder, Lawrence C. Cowsar, and David P. Dobkin. 1998. MAPS: Multiresolution Adaptive Parameterization of Surfaces. In *SIGGRAPH*. ACM, 95–104.

Xianzhi Li, Ruihui Li, Lei Zhu, Chi-Wing Fu, and Pheng-Ann Heng. 2020. DNF-Net: a Deep Normal Filtering Network for Mesh Denoising. *CoRR* abs/2006.15510 (2020).

Yangyan Li, Rui Bu, Mingchao Sun, Wei Wu, Xinhan Di, and Baoquan Chen. 2018. PointCNN: Convolution On X-Transformed Points. In *NeurIPS*. 828–838.

Chunfeng Lian, Li Wang, Tai-Hsien Wu, Mingxia Liu, Francisca Durán, Ching-Chang Ko, and Dinggang Shen. 2019. MeshSNet: Deep Multi-scale Mesh Feature Learning for End-to-End Tooth Labeling on 3D Dental Surfaces. In *MICCAI (6) (Lecture Notes in Computer Science)*, Vol. 11769. Springer, 837–845.

Isaak Lim, Alexander Dielen, Marcel Campen, and Leif Kobbelt. 2018. A Simple Approach to Intrinsic Correspondence Learning on Unstructured 3D Meshes. In *ECCV Workshops (3) (Lecture Notes in Computer Science)*, Vol. 11131. Springer, 349–362.

Or Litany, Tal Remez, Emanuele Rodolà, Alexander M. Bronstein, and Michael M. Bronstein. 2017. Deep Functional Maps: Structured Prediction for Dense Shape Correspondence. In *ICCV*. IEEE Computer Society, 5660–5668.

Hsueh-Ti Derek Liu, Vladimir G. Kim, Siddhartha Chaudhuri, Noam Aigerman, and Alec Jacobson. 2020. Neural subdivision. *ACM Trans. Graph.* 39, 4 (2020), 124.

Yang Liu, Helmut Pottmann, Johannes Wallner, Yong-Liang Yang, and Wenping Wang. 2006. Geometric modeling with conical meshes and developable surfaces. *ACM Trans. Graph.* 25, 3 (2006), 681–689.

Zheng-Ning Liu, Yan-Pei Cao, Zheng-Fei Kuang, Leif Kobbelt, and Shi-Min Hu. 2021. High-Quality Textured 3D Shape Reconstruction with Cascaded Fully Convolutional Networks. *IEEE Trans. Vis. Comput. Graph.* 27, 1 (2021), 83–97.

Charles Loop. 1987. Smooth Subdivision Surfaces Based on Triangles. *Masters Thesis, Department of Mathematics, University of Utah* (January 1987).

Haggai Maron, Meirav Galun, Noam Aigerman, Miri Trope, Nadav Dym, Ersin Yumer, Vladimir G. Kim, and Yaron Lipman. 2017. Convolutional neural networks on surfaces via seamless toric covers. *ACM Trans. Graph.* 36, 4 (2017), 71:1–71:10.

Jonathan Masci, Davide Boscaini, Michael M. Bronstein, and Pierre Vandergheynst. 2015. Geodesic Convolutional Neural Networks on Riemannian Manifolds. In *ICCV Workshops*. IEEE Computer Society, 832–840.

Daniel Maturana and Sebastian A. Scherer. 2015. VoxNet: A 3D Convolutional Neural Network for real-time object recognition. In *IROS*. IEEE, 922–928.

Dushyant Mehta, Srinath Sridhar, Oleksandr Sotnychenko, Helge Rhodin, Mohammad Shafiei, Hans-Peter Seidel, Weipeng Xu, Dan Casas, and Christian Theobalt. 2017. Vnect: Real-time 3d human pose estimation with a single rgb camera. *ACM Transactions on Graphics (TOG)* 36, 4 (2017), 1–14.

Simone Melzi, Jing Ren, Emanuele Rodolà, Abhishek Sharma, Peter Wonka, and Maks Ovsjanikov. 2019. ZoomOut: spectral upsampling for efficient shape correspondence. *ACM Trans. Graph.* 38, 6 (2019), 155:1–155:14.

Francesco Milano, Antonio Loquercio, Antoni Rosinol, Davide Scaramuzza, and Luca Carlone. 2020. Primal-Dual Mesh Convolutional Neural Networks. In *NeurIPS*.

Federico Monti, Davide Boscaini, Jonathan Masci, Emanuele Rodolà, Jan Svoboda, and Michael M. Bronstein. 2017. Geometric Deep Learning on Graphs and Manifolds Using Mixture Model CNNs. In *CVPR*. IEEE Computer Society, 5425–5434.

Federico Monti, Oleksandr Shchur, Aleksandar Bojchevski, Or Litany, Stephan Günnemann, and Michael M. Bronstein. 2018. Dual-Primal Graph Convolutional Networks. *CoRR* abs/1806.00770 (2018). arXiv:1806.00770

Maks Ovsjanikov, Mirela Ben-Chen, Justin Solomon, Adrian Butscher, and Leonidas Guibas. 2012. Functional maps: a flexible representation of maps between shapes. *ACM Transactions on Graphics (TOG)* 31, 4 (2012), 1–11.

Adrien Poulenard and Maks Ovsjanikov. 2018. Multi-directional geodesic neural networks via equivariant convolution. *ACM Trans. Graph.* 37, 6 (2018), 236:1–236:14.

Charles Ruizhongtai Qi, Hao Su, Kaichun Mo, and Leonidas J. Guibas. 2017a. PointNet: Deep Learning on Point Sets for 3D Classification and Segmentation. In *CVPR*. IEEE Computer Society, 77–85.

Charles Ruizhongtai Qi, Li Yi, Hao Su, and Leonidas J. Guibas. 2017b. PointNet++: Deep Hierarchical Feature Learning on Point Sets in a Metric Space. In *NIPS*. 5099–5108.

Anurag Ranjan, Timo Bolkart, Soubhik Sanyal, and Michael J. Black. 2018. Generating 3D Faces Using Convolutional Mesh Autoencoders. In *ECCV (3) (Lecture Notes in Computer Science)*, Vol. 11207. Springer, 725–741.

Jing Ren, Adrien Poulenard, Peter Wonka, and Maks Ovsjanikov. 2018. Continuous and orientation-preserving correspondences via functional maps. *ACM Trans. Graph.* 37, 6 (2018), 248:1–248:16.

Olaf Ronneberger, Philipp Fischer, and Thomas Brox. 2015. U-Net: Convolutional Networks for Biomedical Image Segmentation. In *MICCAI (3) (Lecture Notes in Computer Science)*, Vol. 9351. Springer, 234–241.

Jean-Michel Roufosse, Abhishek Sharma, and Maks Ovsjanikov. 2019. Unsupervised Deep Learning for Structured Shape Matching. In *ICCV*. IEEE, 1617–1627.

Scott Schaefer, E. Vouga, and Ron Goldman. 2008. Nonlinear subdivision through nonlinear averaging. *Comput. Aided Geom. Des.* 25, 3 (2008), 162–180.

Jonas Schult, Francis Engelmann, Theodora Kontogianni, and Bastian Leibe. 2020. DualConvMesh-Net: Joint Geodesic and Euclidean Convolutions on 3D Meshes. In *CVPR*. IEEE, 8609–8619.

Nicholas Sharp, Yousuf Soliman, and Keenan Crane. 2019. Navigating intrinsic triangulations. *ACM Trans. Graph.* 38, 4 (2019), 55:1–55:16.

Baoguang Shi, Song Bai, Zhichao Zhou, and Xiang Bai. 2015. DeepPano: Deep Panoramic Representation for 3-D Shape Recognition. *IEEE Signal Process. Lett.* 22, 12 (2015), 2339–2343.

Ayan Sinha, Jing Bai, and Karthik Ramani. 2016. Deep Learning 3D Shape Surfaces Using Geometry Images. In *ECCV (6) (Lecture Notes in Computer Science)*, Vol. 9910. Springer, 223–240.

Hang Su, Subhransu Maji, Evangelos Kalogerakis, and Erik G. Learned-Miller. 2015. Multi-view Convolutional Neural Networks for 3D Shape Recognition. In *ICCV*. IEEE Computer Society, 945–953.

Maxim Tatarchenko, Jaesik Park, Vladlen Koltun, and Qian-Yi Zhou. 2018. Tangent Convolutions for Dense Prediction in 3D. In *CVPR*. IEEE Computer Society, 3887–3896.

Petar Velickovic, Guillem Cucurull, Arantxa Casanova, Adriana Romero, Pietro Liò, and Yoshua Bengio. 2018. Graph Attention Networks. In *ICLR (Poster)*. OpenReview.net.

Daniel Vlasic, Ilya Baran, Wojciech Matusik, and Jovan Popovic. 2008. Articulated mesh animation from multi-view silhouettes. *ACM Trans. Graph.* 27, 3 (2008), 97.

Nanyang Wang, Yinda Zhang, Zhuwen Li, Yanwei Fu, Wei Liu, and Yu-Gang Jiang. 2018. Pixel2Mesh: Generating 3D Mesh Models from Single RGB Images. In *ECCV (11) (Lecture Notes in Computer Science)*, Vol. 11215. Springer, 55–71.

Peng-Shuai Wang, Yang Liu, Yu-Xiao Guo, Chun-Yu Sun, and Xin Tong. 2017. O-CNN: octree-based convolutional neural networks for 3D shape analysis. *ACM Trans. Graph.* 36, 4 (2017), 72:1–72:11.

Yunhai Wang, Shmulik Asafi, Oliver van Kaick, Hao Zhang, Daniel Cohen-Or, and Baoquan Chen. 2012. Active co-analysis of a set of shapes. *ACM Trans. Graph.* 31, 6 (2012), 165:1–165:10.

Yue Wang, Yongbin Sun, Ziwei Liu, Sanjay E. Sarma, Michael M. Bronstein, and Justin M. Solomon. 2019. Dynamic Graph CNN for Learning on Point Clouds. *ACM Trans. Graph.* 38, 5 (2019), 146:1–146:12.

Zhirong Wu, Shuran Song, Aditya Khosla, Fisher Yu, Linguang Zhang, Xiaoou Tang, and Jianxiong Xiao. 2015. 3D ShapeNets: A deep representation for volumetric shapes. In *CVPR*. IEEE Computer Society, 1912–1920.

Yun-Peng Xiao, Yu-Kun Lai, Fang-Lue Zhang, Chunpeng Li, and Lin Gao. 2020. A survey on deep geometry learning: From a representation perspective. *Comput. Vis. Media* 6, 2 (2020), 113–133.

Haotian Xu, Ming Dong, and Zichun Zhong. 2017. Directionally Convolutional Networks for 3D Shape Segmentation. In *ICCV*. IEEE Computer Society, 2717–2726.

Li Yi, Hao Su, Xingwen Guo, and Leonidas J. Guibas. 2017. SyncSpecCNN: Synchronized Spectral CNN for 3D Shape Segmentation. In *CVPR*. IEEE Computer Society, 6584–6592.

A FURTHTER DETAILS ON REMESHING

To construct the subdivision sequence connectivity, the MAPS algorithm [Lee et al. 1998] establishes a bijective map between the raw mesh and its decimated version. In detail, MAPS iteratively removes the maximum independent set of the vertices. When a vertex is removed, MAPS first re-triangulates the 1-ring neighbors, and calculates a conformal map over the local region between before

and after the removal. The removed vertices are also parameterized on the decimated mesh. After the raw mesh has been simplified onto a base mesh, a global parameterization is constructed. Then Loop subdivision [Loop 1987] without vertex update is applied to the base mesh d times, where d is the subdivision depth, and the vertices of the subdivided mesh are projected onto the raw mesh using the global parameterization. Because the global parameterization is between the raw mesh and the simplified mesh, this idea is also called *self-parameterization*. One obvious advantage of MAPS is that it supports any genus as long as the decimation process does not break the topology.

Recently [Liu et al. 2020] propose a modified MAPS method, utilizing an edge collapse based decimation, e.g. qslim [Garland and Heckbert 1997], rather than vertex removal, which improves the decimation quality.

In practice, we find both methods have limitations. In MAPS, the order of vertex removal is crucial. For example, repeated removal of limb vertices in the mesh of a horse will lead to insufficient sampling of the limbs in the outputs, and ultimately the hooves cannot be fully reconstructed. This causes significant distortion if the mesh contains small but important details (see Fig. 6). Liu et al. [2020] tackle the issue with a better decimation algorithm and prohibit collapse that causes poor quality of triangles. However, the latter also restricts the lowest base size the algorithm can reach (see Fig. 7).

More importantly, there exists the possibility of *UV flip*, so that a triangle face on the original mesh cannot be mapped to a triangular region in the parameter domain. Sampling on flipped *UV* triangles may lead to failures of remeshing. In detail, when removing a vertex, MAPS first flattens the vertex and its one-ring neighbors. The flattening, or local parameterization, may be invalid because of *UV* flip (Fig. 12 (a) shows a case). Because global parameterization is the composition of a sequence of local parameterizations, there will more probably be flip *UV* triangles when the base size is lower. Fortunately, *UV* flip does not occur if the three vertices lie in the same face of the current decimated mesh. Thus to avoid *UV* flip, during decimation and parameterization, we split problematic triangles along with the triangulation of the current decimated mesh. For example, in Fig. 12(b), the triangle with three blue vertices is divided into three smaller triangles as it crosses an edge of the simplified mesh.

However, Liu et al. [2020] do not solve this issue. Instead if *UV* flip occurs after collapsing an edge and parameterizing the related region, they simply abandon this edge collapse operation and move to the next candidate edge to be collapsed. However, as more vertices of the raw mesh are parameterized to the simplified mesh, *UV* flip may become inevitable if the input mesh is over-decimated. Yet, in 2D CNNs, the size of the feature map of the last layer is often very small, e.g. 7×7 pixels in ResNet [He et al. 2016]. Thus, for some inputs, Liu et al.'s method cannot meet our requirements.

B MANIFOLD40

We employed a reconstruction algorithm [Huang et al. 2018] to make the models in ModelNet40 watertight. This method constructs an octree for the shape, extracts isosurfaces, and projects vertices onto the original shape. Small and isolated components are cleaned after
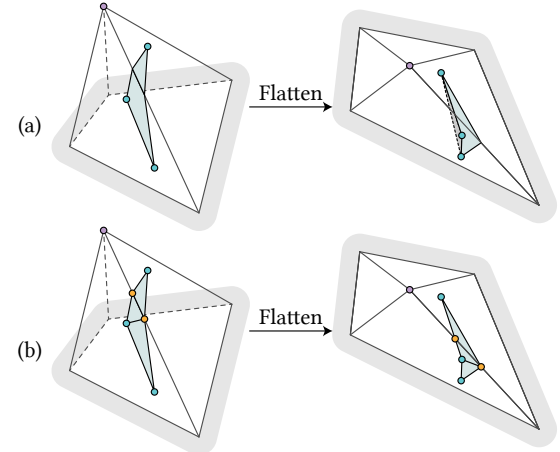
Fig. 12. *UV* Flip. (a) Example of *UV* flip after local parameterization. The three blue vertices form a face in the input mesh, already removed in earlier steps. Now they are parameterized in the current simplified mesh. (b). Splitting the blue triangle into three triangles with orange vertices prevents the problem.

Fig. 13. Examples from Manifold40.

reconstruction. Sometimes, we found that non-manifold vertices might exist; we split these vertices using MeshLab [Cignoni et al. 2008]. Following the datasets contributed by [Hanocka et al. 2019], all meshes were simplified to contain exactly 500 faces. Simplifying meshes also speeds the remeshing process. Fig. 13 illustrates some examples from Manifold40.

We found some shapes in Manifold40 to have a genus larger than 20. Because the decimation process of remeshing does not change the topology of shapes, it is almost impossible to reach a base size of 48 for such shapes. Therefore, we chose a more tolerant strategy: the base size of most meshes is enlarged to 96, and shapes with complicated topology are decimated as little as possible. As a result, except for 11 training samples, the base size of all other meshes was between 96 and 192. We simply discarded those 11 samples when training SubdivNet. To avoid heavy demands on computational resources, the depth was reduced to 3 from 4.

Using variable base sizes leads to variable input sizes. To incorporate them in a conventional batch-based training scheme, we padded meshes with empty faces to guarantee all inputs have the same size in a mini-batch. Because the global pooling layer after

Table 11. Mesh segmentation accuracy using MeshCNN's metric.

Method	HumanBody	coseg aliens
MeshCNN [Hanocka et al. 2019]	92.3%	97.6%
MeshWalker [Lahav and Tal 2020]	94.8%	99.1%
SubdivNet	**96.6**%	**99.4**%

convolutions does not restrict the mesh to have a fixed number of faces, SubdivNet can be trained and evaluated with variable input sizes.

C SEGMENTATION ACCURACY USING MESHCNN'S METRIC

When evaluating segmentation results, MeshCNN first simplified the input meshes, and then used a simple criterion to calculate accuracy using the edges of the simplified meshes: the prediction of an edge is correct if either endpoint is correct. We also projected our segmentation results to the edges of MeshCNN's simplified dataset using the nearest strategy. Table 11 suggests that SubdivNet is also superior to other methods using this evaluation metric.